Journal of Power Sources 206 (2012) 282–287

Contents lists available at SciVerse ScienceDirect

Journal of Power Sources

journal homepage: www.elsevier.com/locate/jpowsour

Electrochemical performance of the nanostructured biotemplated V_2O_5 cathode for lithium-ion batteries

Ekaterina Pomerantseva[a,b,*], Konstantinos Gerasopoulos[a,b,c], Xinyi Chen[c], Gary Rubloff[b,c], Reza Ghodssi[a,b,c,**]

[a] MEMS Sensors and Actuators Laboratory (MSAL), Department of Electrical and Computer Engineering, University of Maryland, College Park, MD 20742, USA
[b] Institute for Systems Research, University of Maryland, College Park, MD 20742, USA
[c] Department of Materials Science and Engineering, University of Maryland, College Park, MD 20742, USA

ARTICLE INFO

Article history:
Received 24 November 2011
Received in revised form 20 January 2012
Accepted 21 January 2012
Available online 28 January 2012

Keywords:
Lithium-ion battery
Vanadium oxide
Cathode material
Tobacco mosaic virus template
Nanostructuring

ABSTRACT

We report for the first time fabrication of nanostructured V_2O_5 thin film cathodes for lithium-ion batteries using *Tobacco mosaic virus* (*TMV*) particles as biological templates. *TMV*-templated V_2O_5 electrodes showed enhanced electrochemical performance compared to electrodes with a planar configuration demonstrating high specific capacity, excellent rate capability and cycling stability. A specific capacity of 12 $\mu Ah\,cm^{-2}$ was achieved for the *TMV*-templated electrode with a V_2O_5 layer thickness of ~30 nm, which is 7–8 times higher than the specific capacity of planar V_2O_5 electrodes of the same thickness. Higher areal specific capacities are achievable by increasing active battery material loading: electrodes with twice higher V_2O_5 loading delivered capacities of ~25 $\mu Ah\,cm^{-2}$. Development of the cathode is an important step towards the fabrication of rechargeable lithium-ion batteries with superior virus-templated electrodes for high performance electrochemical energy storage.

1. Introduction

Lithium-ion batteries are currently attracting considerable attention as power sources for a variety of devices, ranging from consumer electronics and electric vehicles to military and aerospace applications, due to their higher energy density compared to other systems [1–3]. This attribute is particularly important for the widespread commercialization of miniaturized next-generation devices and systems such as implantable microsensors and microactuators as well as wireless sensor networks, the use of which is currently limited by the low energy and power densities of traditional planar (2D) thin film technologies [4]. As a result, significant research efforts have been focused on the development of novel material synthesis and device fabrication techniques that can provide the desirable energy and power levels for the reliable operation of such devices.

Nanostructured materials have emerged as a promising solution in this direction due to significant benefits they offer compared to the bulk counterparts, such as higher electrode/electrolyte contact areas, improved mechanical stability, as well as reduced distances for electron and ion transport that enable faster reaction kinetics [1–3]. Among synthetic approaches developed to obtain nanostructured materials, template-based synthesis has been commonly used since it allows fabrication of uniform arrays of various materials. In particular, the use of porous membranes combined with material deposition techniques has been an effective method for the fabrication of nanostructured electrodes for Li-ion batteries with improved electrochemical performance [5–9]. For example Martin and co-worker [5] synthesized V_2O_5 nanorods using sol–gel deposition in polycarbonate (PC) membranes, while Cao and co-workers [8] used PC membranes to electrodeposit Ni nanorods which acted as current collectors followed by the sol–gel deposition of V_2O_5 active material. While these approaches generally demonstrate the merits of using nanostructured electrodes compared to planar thin-films, the methods used for nanowire synthesis are not easily scalable to complex geometries or wafer level processes.

In addition to traditional template-based fabrication techniques, notable research interest has been directed towards the use of biological particles as templates for the synthesis of inorganic nanostructures [10]. Molecules such as peptides, DNA and viruses

* Corresponding author at: MEMS Sensors and Actuators Laboratory (MSAL), Department of Electrical and Computer Engineering, Institute for Systems Research, University of Maryland, College Park, MD 20742, USA. Tel.: +1 301 405 2168; fax: +1 301 314 9920.
** Corresponding author at: MEMS Sensors and Actuators Laboratory (MSAL), Department of Electrical and Computer Engineering, Institute for Systems Research, Department of Materials Science and Engineering, University of Maryland, 2173 A.V. Williams Building, College Park, MD 20742, USA. Tel.: +1 301 405 8158; fax: +1 301 314 9920.
E-mail addresses: epomeran@umd.edu (E. Pomerantseva), ghodssi@umd.edu (R. Ghodssi).

0378-7753/$ – see front matter © 2012 Elsevier B.V. All rights reserved.
doi:10.1016/j.jpowsour.2012.01.127

exhibit several added benefits including simplicity, low cost, surface tunability as well as the ability to create monodisperse, well ordered architectures. Approaches that utilize the shape of these molecules [11] and/or biologically engineered chemical functionalities in their structure [12–14] have been previously reported for the synthesis of lithium-ion battery anodes and cathodes. These biotemplated nanostructures cannot be synthesized directly on current collectors however and have to be mixed with binders and conductive additives to form electrodes with traditional ink-casting techniques.

Previous work led by our group has been focused on the use of *Tobacco mosaic virus* (*TMV*) particles as scaffolds for the synthesis of energy related nanostructures [15,16]. The *TMV* is a plant virus with a cylindrical, rod-like structure which can be genetically modified with cysteine functional groups that facilitate electroless nickel plating as well as self-assembly of the molecules onto various substrates. Unlike other biologically inspired methods, the unique characteristics of this approach lie in the self-assembly of the *TMV*, which enables direct synthesis of the electrodes onto current collectors without the use of binders and other additives. In addition, the robustness of the structures following metallization allows combination of the bottom-up self-assembly with standard microfabrication processes such as thin film deposition techniques, photolithographic patterning and three-dimensional (3D) micro/nano structure fabrication [17]. Consequently, this technology can alleviate limitations involved in other surface-attached nanorod methods [5–9] that cannot be easily expanded or scaled to more complex planar and 3D geometries. Recently, the fabrication of Li-ion battery anodes such as Si and TiO_2 using a core/shell nanoarchitecture was demonstrated [18–21]. In these electrodes, the electroless deposited metal layer serves as the current collector and 3D support, while the active material is deposited using physical vapor deposition, electroplating, or atomic layer deposition (ALD) on the virus-structured nanonetwork. These electrodes exhibited high specific capacities, excellent cyclic stability and rate performance as a result of this self-assembled, core/shell nanostructure.

The work presented here is focused on the development of a *TMV*-templated cathode using the established synthetic route. The active material selected is V_2O_5, a widely explored cathode material that can react with more than one lithium per redox ion, resulting in electrodes with high specific energy and capacity [22,23]. Specifically, V_2O_5 is deposited onto the nickel-coated *TMV* using a novel ozone-based ALD process, a technique very suitable for the synthesis of thin nanolayers with precise control over thickness and uniformity [24,25]. In addition, this ozone-based ALD method produces crystalline V_2O_5 without the need for post deposition annealing. The development of a high performance cathode, combined with the previously developed anodes as well as the device patterning capabilities of the *TMV*-templated materials, will enable the fabrication of fully virus-structured microbatteries. Moreover, this biotemplating nanostructuring approach marks an advance in the design of lithium-ion battery electrodes and can serve as the inspiration for future electrode materials for macro-scale applications.

2. Experimental

The nanostructured *TMV*-templated Ni/V_2O_5 electrodes were fabricated on stainless steel discs (15.5 mm diameter, Pred Materials International, USA) with a sputter-deposited Au layer that facilitates more efficient *TMV* self-assembly. The nickel-coated *TMV* core of the electrodes was synthesized as previously described [15,21]. Briefly, the stainless steel discs were first immersed in sodium phosphate buffer solution at pH 7, containing *TMV* at a concentration of 0.2 g L^{-1}. The substrates were allowed to incubate overnight to maximize *TMV* assembly. Next, the discs were immersed in a solution containing phosphate buffer and sodium tetrachloropalladate ($NaPdCl_4$, 98%, Sigma–Aldrich, MO, USA) in a 12:1 ratio for 2–3 h. During this stage, the *TMV* surface is functionalized with Pd nanoclusters. Finally, nickel is deposited from the electroless plating bath. The stock solution (25 ml) is prepared by mixing 0.6 g nickel chloride ($NiCl_2$, 99%, Sigma–Aldrich, MO, USA), 0.45 g glycine (tissue grade, Fischer Scientific, PA, USA), 1.5 g sodium tetraborate ($Na_2B_4O_7$, 99%, Sigma–Aldrich, MO, USA) and 0.77 g dimethylamine borane (DMAB, 97%, Sigma–Aldrich, MO, USA). This solution is mixed with DI water in a 1:1 ratio and chips are immersed in the bath for 3–5 min. Nickel is initially deposited onto the Pd catalyzed sites and then the reaction proceeds autocatalytically to form a uniform 20–30 nm Ni coating on the *TMV* rod. For comparison, planar electrodes without *TMV* were synthesized onto steel disc substrates, covered with the electroless deposited nickel layer.

Deposition of V_2O_5 was performed in a BENEQ TFS 500 ALD reactor by alternate pulses of vanadium triisopropoxide (VTOP) and ozone at 170 °C. A MKS O3MEGA™ ozone delivery subsystem was employed to supply a stable 18 wt% flow of O_3 from pure O_2 source. The V_2O_5 deposition rate was measured to be 0.03 nm/cycle (where a cycle denotes one sequence of precursor pulses and purging pulses in the ALD reactor). The V_2O_5 was deposited for 1000 and 2000 ALD cycles, aiming at target thicknesses of 30 nm and 60 nm respectively. The mass of the active material was determined by weight measurements with a high precision microbalance (Mettler Toled, XS105 dualRange, 1 μg) before and after V_2O_5 deposition.

The electrode morphology was analyzed using scanning electron microscopy (Hitachi SU-70 HR-SEM). The structural features and composition of the electrode materials were investigated using transmission electron microscopy (JEOL 2100F field emission TEM) with energy-dispersive X-ray spectroscopy (EDS). Phase identification was carried out by X-ray powder diffraction experiments on a Brucker D8 Advance powder diffractometer equipped with LynxEye PSD detector and Ni β-filter using CuKα radiation (step size 0.02° in the range of $14° < 2\theta < 55°$). Electrochemical experiments were carried out in the half-cell configuration assembled in standard coin cells (R032). *TMV*-templated as well as planar Ni/V_2O_5 electrodes served as the cathode, metallic lithium (Sigma–Aldrich, MO, USA) pressed against a stainless steel disc served as the anode, while a Celgard separator (Celgard® 3501) was placed between the two electrodes and soaked with the electrolyte (1 M $LiPF_6$ solution in ethyl carbonate/diethylcarbonate (EC/DEC, 1:1), Novolyte Technologies, OH, USA). Cell assembly was performed in a glove box with oxygen concentration of less than 0.2 ppm and Argon as the carrier gas. Galvanostatic experiments were carried out using a multiple channel battery test station (Arbin Instruments, TX, USA) while cyclic voltammetry scans were obtained using a Gamry G750 series potentiostat (Gamry Instruments, PA, USA), both in the 2.6–4.0 V range.

3. Results and discussion

Fig. 1 shows the morphology and composition of *TMV*-templated Ni/V_2O_5 electrodes. The SEM image (Fig. 1a) reveals that nickel coated *TMV* templates attach to the Au-coated stainless steel surface with a preferred vertical orientation, in agreement with the previous studies [17–21]. The leaning and bending of virus molecules arise from the roughness of the stainless steel disk surface and flexibility of the TMV molecule itself. TMV particles tend to self-align (usually, up to three molecules form a pseudo-wire) producing a continuous layer made of interwoven fibers with the length of ~900 nm. The cross-section TEM image (Fig. 1b) demonstrates a layered structure for a single virus-templated particle. EDS line-scanning elemental mapping (Fig. 1b, inset) of Ni and V revealed that the Ni profile showed a peak that was located

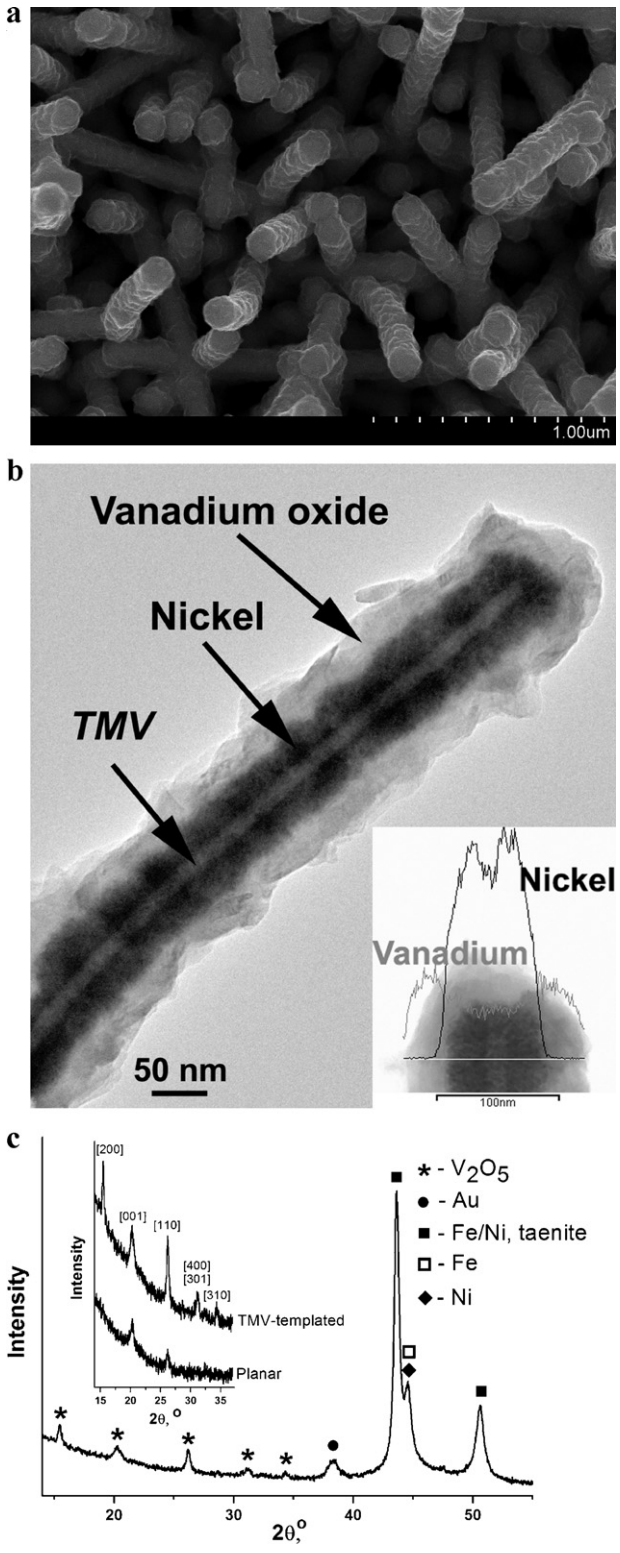

Fig. 1. Morphology and phase composition of the *TMV*-templated Ni/V_2O_5 core/shell cathode. (a) SEM image of the cathode fabricated on the Au-coated stainless steel disk; (b) TEM image of a single composite nanowire (inset shows EDX line scan elemental mapping indicating the Ni and V elemental profiles across the nanowire); (c) XRD pattern of the TMV-templated V_2O_5 cathode shown in (a): V_2O_5, Au and stainless steel (Fe, Ni, Fe/Ni) reflections are indicated (inset shows an expanded region with V_2O_5 reflections and corresponding Miller indexes for both planar and TMV-templated V_2O_5 electrodes).

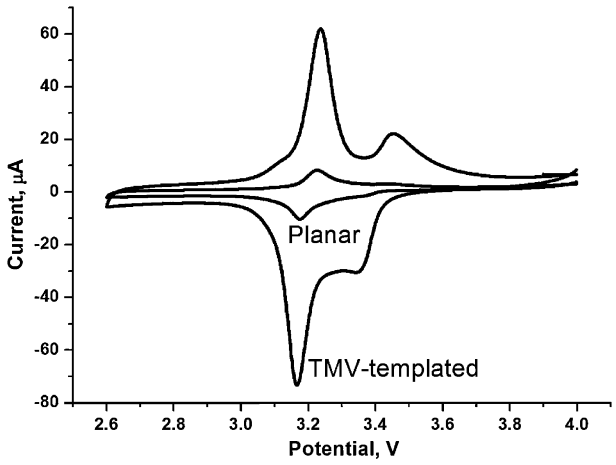

Fig. 2. Cyclic voltammograms (second cycle) of the V_2O_5/Li cells with planar and *TMV*-templated electrodes in a voltage window of 2.6–4.0 V at a sweep rate of 0.2 mV s^{-1}.

at the center of the V profile; this corresponds to the core/shell configuration of the nanocomposite particle. The nickel metal layer has a thickness of ~30 nm and uniformly covers the *TMV* particle. The role of the Ni is to serve as a current collector and enable rigidity of the biological templates in the electrodes. The nickel core provides a highly electron conductive path for every nanowire, which enhances the rate capability of *TMV*-templated lithium-ion battery electrodes. The V_2O_5 layer (~30 nm thick) was uniformly deposited on top of the Ni using the ozone-based ALD process. ALD is unique in producing thin nanolayers of materials, thus maintaining the high surface area of the electrodes established by self-assembled *TMV* templates. The typical mass of V_2O_5 on *TMV*-coated 15.5 mm Ø disk was ~0.160 mg. The mass ranged from 0.140 to 0.180 mg; the variation in mass depends on the virus coverage of the substrate and as result on the surface area available for the active battery material deposition. For comparison, the mass of V_2O_5 deposited on a planar Ni-coated stainless steel disk with the same geometry was ~0.027 mg, ranging from 0.024 to 0.031 mg. This six to eightfold increase in active material loading for the *TMV*-templated electrodes is directly linked with the increase in surface area due to the viral nanostructures, since ALD can produce uniform thin coatings across the whole electrode surface that is exposed to the precursors.

Using ozone as the oxidizing agent results in well crystallized V_2O_5 films without post-ALD annealing which is advantageous compared to the traditionally used H_2O-based V_2O_5 ALD that produces amorphous films [24,25]. The XRD patterns for a V_2O_5 film deposited on planar and *TMV*-coated stainless steel disks are shown in Fig. 1c. The V_2O_5 ALD film crystallizes in the orthorhombic cell (JSPDS No. 41-1426) and exhibits a high preferred orientation along the *c* axis, as evident by the strong intensity of the (0 0 1) line in the XRD pattern of the planar V_2O_5 film (Fig. 1c, inset). Interestingly additional (*h k l*) lines become visible in the XRD pattern of the *TMV*-templated V_2O_5 electrode (Fig. 1c, inset). This is attributed to the vertical orientation of the viral molecules on the Au coated stainless steel substrates which cancels preferred orientation effect observed for planar V_2O_5 films.

The electrochemical properties of lithium ion intercalation/deintercalation into and out of the *TMV*-templated V_2O_5 film electrodes have been investigated in half-cell coin batteries. For comparison, V_2O_5 electrodes with a planar configuration have been studied under the same conditions. Cyclic voltammogram (CV) curves for the V_2O_5 electrodes are shown in Fig. 2. They demonstrate two peaks at ~3.16 and ~3.35 V which result from the Li^+ intercalation process in the reduction cycle, and two corresponding peaks at ~3.23 and ~3.45 V in the oxidation cycle, indicating

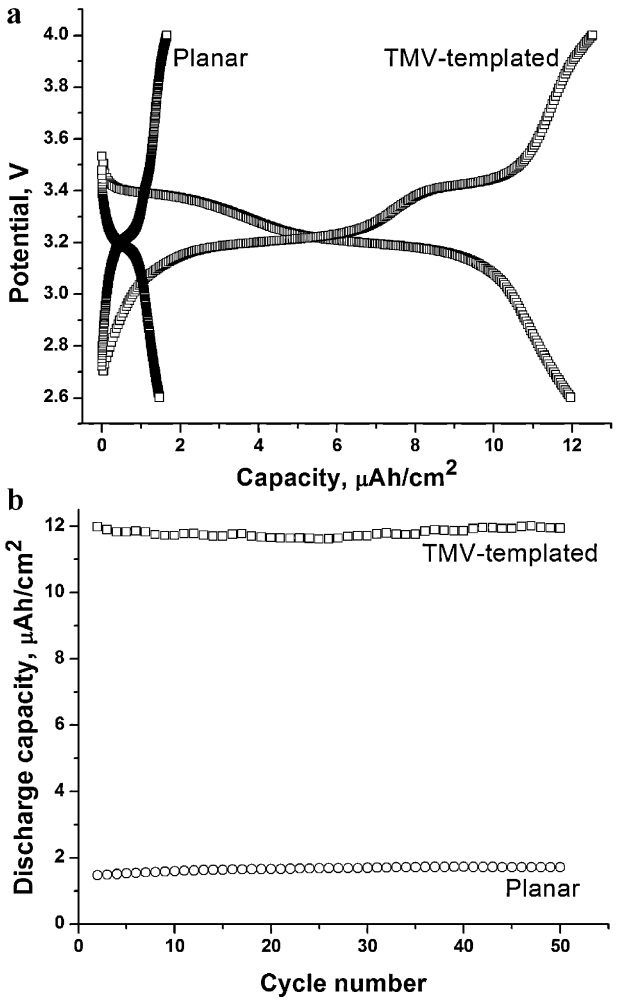

Fig. 3. (a) Discharge and charge curves (second cycle) and (b) the cycling performance of the cells with planar and *TMV*-templated V_2O_5 electrodes in the voltage range of 2.6–4.0 V at a current density of 5 μA cm^{-2}.

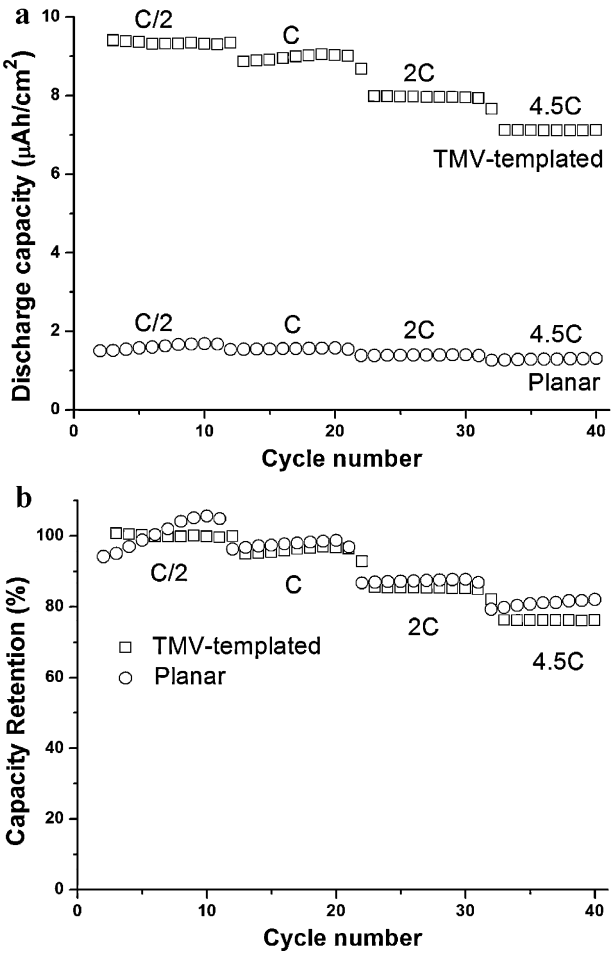

Fig. 4. Rate capability data for planar and *TMV*-templated V_2O_5 electrodes in the voltage range of 2.6–4.0 V at different C-rates indicated in the figure. (a) Discharge capacity and (b) capacity retention vs. cycle number. The capacity retention is presented based on the ratio C_i/C_{av}, where C_i is the capacity for each cycle, and C_{av} is the average capacity for the initial lowest *C*-rate.

Li^+ deintercalation. The area under these peaks on the CV curve is notably higher for the *TMV*-templated electrode compared to that for the planar thin film. This is attributed to the higher surface area of the nanostructured virus-templated V_2O_5 electrode and higher mass loading of the active battery material.

Fig. 3a demonstrates discharge/charge curves of the cells with planar and *TMV*-templated V_2O_5 electrodes at the second cycle in the voltage range of 2.6–4.0 V. Two distinct voltage plateaus are observed on both discharge and charge curves for both electrodes, in good agreement with the CV data (Fig. 2) and literature [22,23]. The capacity of the *TMV*-templated V_2O_5 electrodes (12 μAh cm^{-2}) is 8 times higher than the capacity of the planar electrode (1.5 μAh cm^{-2}), which is consistent with the mass difference as indicated previously. Higher capacity of the nanostructured virus-templated V_2O_5 is achieved due to the higher surface area of the electrode, in accordance with the previously estimated increase in surface area for the *TMV* templates compared to planar surfaces [10]. It should be noted that both current density and capacity values in this work are normalized over the footprint area of the steel disc electrode, since the limiting factors in microbattery development are the available areal footprint for the power source, as well as the current required for each particular application. This makes the areal capacity the important figure of merit for microbattery performance characterization, as described in previous work [4]. The gravimetric capacity of both electrodes at a current density of 5 μA cm^{-2} is ~128–130 mAh g^{-1}, which is comparable to the theoretical capacity of V_2O_5 in the potential window of 2.6–4.0 V (147 mAh g^{-1} [22]). Fig. 3b shows that the specific capacities demonstrated by the *TMV*-templated 30 nm thick V_2O_5 electrodes during extended cycling test are consistently higher than those delivered by planar V_2O_5 electrodes with the same thickness. At a current density of 5 μA cm^{-2}, a specific capacity of ~12 μAh cm^{-2} is obtained for *TMV*-templated electrodes without significant fading over 50 cycles (Fig. 3b), indicating excellent cycling stability of the active electrode material.

Fig. 4 shows results from rate capability experiments for both *TMV*-templated and planar V_2O_5 electrodes with the same thickness of vanadium oxide (30 nm) upon cycling at different C-rates: C/2, C, 2C and 4.5C. At each current rate, the battery was tested for 10 cycles to ensure the reliability of the reported readings. The specific capacity was stable at a constant current rate, while changes in current density resulted in stepwise dependence of the specific capacity on cycle number, demonstrating capacity drops when the current density was increased. The capacity retention was normalized by the average capacity value at a slowest current rate used in this experiment (C/2). The specific capacity of the *TMV*-templated electrodes is consistently higher than that of the planar electrodes at all current rates used in the experiment (Fig. 4a). At the same time the capacity retention is similar for both types of electrodes (Fig. 4b)

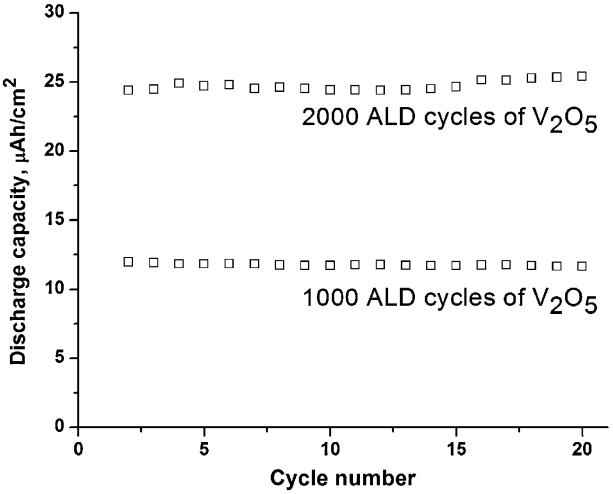

Fig. 5. The cycling performance of the cells with *TMV*-templated electrodes obtained using 1000 and 2000 ALD cycles of V_2O_5 (the thickness of V_2O_5 films is ~30 and ~60 nm, respectively) in the voltage range of 2.6–4.0 V at a current density of 5 μA cm^{-2}.

indicating similarly fast kinetics. This behavior is expected since the active V_2O_5 layer in both electrodes is equally thin (30 nm).

The areal specific capacity of *TMV*-templated electrodes for Li-ion microbatteries can be further improved by increasing the mass loading of the active battery material which is achieved by longer deposition times during ALD process. Fig. 5 shows cycling performance of the *TMV*-templated V_2O_5 electrodes obtained using 1000 and 2000 (typical mass of V_2O_5 was ~0.370–0.400 mg) ALD cycles. *TMV*-templated electrodes obtained using 2000 cycles of V_2O_5 deposition delivered capacities ~25 μAh cm^{-2} which is twice higher than those obtained for the electrodes with 1000 cycles of V_2O_5 ALD, in agreement with the mass difference of active battery material. For comparison, specific capacity of 22 μAh cm^{-2} was reported for 0.6 μm thick planar V_2O_5 film obtained by radio-frequency (RF) magnetron sputtering during the first discharge down to 2.8 V at a C/5 current rate with liquid electrolyte (1 M $LiClO_4$ in propylene carbonate) [21]. In our work, *TMV*-templated ~60 nm thick V_2O_5 electrodes delivered even higher capacities (~25 μAh cm^{-2}) at similar current rates (the current rate of 5 μA cm^{-2} used in the experiment corresponds to ~53 mA g^{-1} which in turn corresponds to ~C/3 in the 2.6–4.0 V potential range for V_2O_5). In addition, thinner active material layers are characterized by shorter electron and ion diffusion distances, and therefore exhibit faster reaction kinetics compared to thicker films, as was previously demonstrated in [21]. These two effects combined clearly illustrate a major advantage of the nanostructuring approach, since similar capacity values can be achieved for a 10 times thinner *TMV*-templated V_2O_5 film.

Improved electrochemical performance for nanoarchitectured V_2O_5 electrodes compared to planar films has been demonstrated previously for nanowire arrays obtained using PC membrane template-based synthesis [5]. In this work, the total mass of both sample types was kept the same and electrodes were cycled at various C-rates. Due to the larger thicknesses required for planar films which limits kinetics at fast rates, capacities were significantly lower at higher C-rates. Based on testing parameters, nanostructured electrodes achieved maximum capacities on the order of 10 μAh cm^{-2} at C/20 rate. In the current work, comparable or higher capacities were obtained. Our testing approach was aimed at analyzing the behavior of electrodes with identical thickness instead of identical mass. Since thicknesses are kept on the same range, rate capabilities are similar; however, as demonstrated in Fig. 4, the *TMV*-templated electrodes delivered a consistent sevenfold increase in energy storage capacity, due to the higher mass. This demonstrates the capability of the *TMV*-templating approach to increase energy density without compromising in power density and rate capability, which has been identified previously as a performance limitation in thin-film microbattery architectures [26]. In addition, in our approach the specific capacity of the electrodes can be easily scaled up by increasing the amount of active battery material using longer deposition times (Fig. 5). These results combined with the patterning and 3D self-assembly capabilities of the viral template highlight the significant benefits of our approach in synthesizing nanostructured microbattery electrodes with complex geometries on various substrates.

The high capacity values, excellent cycling stability and rate capability of the *TMV*-templated V_2O_5 cathodes in lithium-ion batteries can be achieved due to the large surface area and short diffusion distances typical of nanostructured materials. The technology used for the fabrication of V_2O_5 electrodes combines biotemplating and nanostructuring approaches, leading to the increase of the active surface area of *TMV*-templated battery electrodes as compared to their planar analogues. As a result, the electrochemically active material loading is increased without increasing areal footprint, enabling the higher energy density. Moreover, the use of nanostructured materials creates a larger electrode/electrolyte interface and reduces ion diffusion paths improving the power density. In our approach, the electrodes are based on self-assembly of the viral templates onto the current collector without the use of binders and other conductive additives, reducing the fabrication complexity. These results, combined with the previous studies on virus-structured anodes and the patterning capabilities of the *TMV* in microfabricated architectures, demonstrate the feasibility of developing compact, high performance microbatteries with *TMV*-templated nanostructured electrodes. Our current work is focused on the fabrication of hierarchical three-dimensional electrodes composed of gold micropillars coated with the *TMV* particles [27] which can further improve electrochemical performance of microbatteries.

4. Conclusions

Our group has previously demonstrated a library of *TMV*-templated materials for lithium-ion battery anodes. To enable the realization of a fully virus-structured microbattery using this biotemplating nanostructuring approach, it is important to develop *TMV*-templated cathodes. In this work, we have used, for the first time, *TMV* molecules to successfully fabricate nanostructured biotemplated V_2O_5 cathodes for lithium-ion microbatteries with advanced electrochemical performance. Comparison with planar V_2O_5 electrodes shows higher capacities per electrode footprint area for the *TMV*-templated architectures as well as excellent cycling stability and rate capability. The eightfold increase in capacity exhibited by the TMV templated electrodes compared to planar thin films is in close agreement with the estimated increase in surface area reported previously by our team. This improved performance is extremely important for the development of next-generation lithium-ion batteries for autonomous portable microdevices. *TMV*-templated nanostructured V_2O_5 electrodes delivered similar specific capacities compared to 10 times thicker planar V_2O_5 films obtained by RF sputtering. The elegant way to form current collector by electroless nickel plating on the surface of self-assembled *TMV* molecules allows for high performance electrodes fabrication without binders or other additives. The presented approach demonstrates a new direction for the design of nanostructured electrodes for lithium-ion batteries. Finally, this work enables the future development of the

lithium-ion microbattery with both *TMV*-templated nanostructured electrodes.

Acknowledgements

This work was supported by the Laboratory for Physical Sciences, NSF Nanomanufacturing Program (NSF-CMMI 0927693), Maryland TEDCO and Department of Energy (FG0202ER45975). E.P. and X.C. were supported as part of the Nanostructures for Electrical Energy Storage, an Energy Frontier Research Center funded by the U.S. Department of Energy, Office of Science, Office of Basic Energy Sciences under Award Number DESC0001160. The authors acknowledge the staff at Maryland Nanocenter and Dr. Li-Chung Lai at the NISP Lab for assisting with TEM imaging. Also, the authors would like to thank our colleagues at the University of Maryland, Professor Peter Kofinas for providing access to a high precision microbalance, Professor Chunsheng Wang for granting access to the argon-filled glove box, and Professor James Culver for providing us with Cys-modified *TMV* templates.

References

[1] J.M. Tarascon, M. Armand, Nature 414 (2001) 359–367.
[2] A.S. Arico, P. Bruce, B. Scrosati, J.-M. Tarascon, W. van Schalkwijk, Nat. Mater. 4 (2005) 366–377.
[3] M. Armand, J.M. Tarascon, Nature 451 (2008) 652–657.
[4] J.W. Long, B. Dunn, D.R. Rolison, H.S. White, Chem. Rev. 104 (2004) 4463–4492.
[5] C.J. Patrissi, C.R. Martin, J. Electrochem. Soc. 146 (1999) 3176–3180.
[6] N. Li, C.R. Martin, B. Scrosati, Electrochem. Solid-State Lett. 3 (2000) 316–318.
[7] N. Li, C.R. Martin, J. Electrochem. Soc. 148 (2001) A164–A170.
[8] K. Takahashi, Y. Wang, G. Cao, J. Phys. Chem. B 109 (2004) 48–51.
[9] J. Jiang, Y. Li, J. Liu, X. Huang, Nanoscale 3 (2011) 45–58.
[10] N. Ma, E.H. Sargent, S.O. Kelley, J. Mater. Chem. 18 (2008) 954–964.
[11] S.-W. Kim, T.H. Han, J. Kim, H. Gwon, H.-S. Moon, S.-W. Kang, S.O. Kim, K. Kang, ACS Nano 3 (2009) 1085–1090.
[12] Y.J. Lee, H. Yi, W.-J. Kim, K. Kang, D.S. Yun, M.S. Strano, G. Ceder, A.M. Belcher, Science 324 (2009) 1051–1055.
[13] K.T. Nam, D.-W. Kim, P.J. Yoo, C.-Y. Chiang, N. Meethong, P.T. Hammond, Y.-M. Chiang, A.M. Belcher, Science 312 (2006) 885–888.
[14] K.T. Nam, R. Wartena, P.J. Yoo, F.W. Liau, Y.J. Lee, Y.-M. Chiang, P.T. Hammond, A.M. Belcher, Proc. Natl. Acad. Sci. U.S.A. 105 (2008) 17227–17231.
[15] E. Royston, A. Ghosh, P. Kofinas, M.T. Harris, J.N. Culver, Langmuir 24 (2007) 906–912.
[16] K. Gerasopoulos, M. McCarthy, P. Banerjee, X. Fan, J. Culver, R. Ghodssi, J. Micromech. Microeng. 18 (2008) 104003.
[17] K. Gerasopoulos, M. McCarthy, P. Banerjee, X. Fan, J.N. Culver, R. Ghodssi, Nanotechnology 21 (2010) 055304.
[18] X. Chen, K. Gerasopoulos, J. Guo, A. Brown, R. Ghodssi, J.N. Culver, C. Wang, Electrochim. Acta 56 (2011) 5210–5213.
[19] X. Chen, K. Gerasopoulos, J. Guo, A. Brown, C. Wang, R. Ghodssi, J.N. Culver, ACS Nano 4 (2010) 5366–5372.
[20] X. Chen, K. Gerasopoulos, J. Guo, A. Brown, C. Wang, R. Ghodssi, J.N. Culver, Adv. Funct. Mater. 21 (2011) 380–387.
[21] K. Gerasopoulos, X. Chen, J. Culver, C. Wang, R. Ghodssi, Chem. Commun. 46 (2010) 7349–7351.
[22] M.S. Whittingham, Chem. Rev. 104 (2004) 4271–4302.
[23] N.A. Chernova, M. Roppolo, A.C. Dillon, M.S. Whittingham, J. Mater. Chem. 19 (2009) 2526–2552.
[24] J.C. Badot, S. Ribes, E.B. Yousfi, V. Vivier, N. Pereira-Ramos, D. Lincot, Electrochem. Solid-State Lett. 3 (2000) 485–492.
[25] X. Chen, E. Pomerantseva, P. Banerjee, K. Gregorczyk, R. Ghodssi, G. Rubloff, Ozone-based atomic layer deposition of crystalline V2O5 films for high performance electrochemical energy storage, Chem. Mater., submitted for publication.
[26] C. Navone, J.P. Pereira-Ramos, R. Baddour-Hadjean, R. Salot, J. Electrochem. Soc. 153 (2006) A2287–A2293.
[27] K. Gerasopoulos, E. Pomerantseva, M. McCarthy, J. Culver, C. Wang, R. Ghodssi, 16th International Solid-State Sensors Actuators and Microsystems Conference (TRANSDUCERS), Beijing, China, June 5–9, 2011.